PCCP

Accepted Manuscript

ROYAL SOCIETY OF CHEMISTRY

www.rsc.org/pccp

Physical Chemistry Chemical Physics RSCPublishing

ARTICLE

Fine-Tuning Solid-State Luminescence in NPIs (1,8-naphthalimides): Impact of Molecular Environment and Cumulative Interactions

Cite this: DOI: 10.1039/x0xx00000x

Received 00th January 2012,
Accepted 00th January 2012

DOI: 10.1039/x0xx00000x

www.rsc.org/

Sanjoy Mukherjee*, and Pakkirisamy Thilagar*

Abstract: An investigation of a series of seven angular "V" shaped NPIs (**1-7**) are presented. The effect of substitutions of these structurally similar NPIs on their photophysical properties in solution-state and solid-state are presented and discussed in the light of experimental and computational findings. Compounds **1-7** show negligible to intensely strong emission yields in their solid-state depending on the nature of substituents appended with the oxoaryl moiety. The solution and solid-state properties of the compounds can be directly correlated to their structural rigidity, nature of substituents and intermolecular interactions. The versatile solid-state structures of the NPI siblings are deeply affected by the pendant substituents. All of the NPIs (**1-7**) show antiparallel dimeric π-π stacking interactions in their solid-state which can further extend in parallel, alternate, orthogonal or lateral fashion depending on the steric and electronic natures of the C-4' substituents. Structural investigations including Hirsfeld surface analysis methods reveal that where strongly interacting systems show weak to moderate emission in their condensed states, weakly interacting systems show strong emission yields under same conditions. The natures of packing and extended structures also affect the emission colors of the NPIs in their solid-states. Further, DFT computational studies were utilized to understand the molecular and cumulative electronic behaviors of the NPIs. The comprehensive studies provide insight into the condensed-state luminescence of aggregation-prone small molecules like NPIs and help to correlate the structure-property relationships.

Introduction:

The modern applications of organic materials have vastly widened our outlook on organic molecules and their functional opportunities in last few decades.[1] In recent times, organic luminescent materials have made a huge impact on display and lighting technologies owing to the successful commercialization of OLEDs (organic light-emitting diodes).[2] Even till very recent times, the concepts and understanding of luminescence were mostly constrained to the solution-state properties.[3] In only last few years, considerably large attentions have been driven towards the apparently young field of solid-state luminescence.[2,4,13-17] Though the preparation and utilizations of large and macromolecules have opened several unprecedented opportunities in this field, low molecular weight small molecules have their certain advantages which cannot be obtained otherwise. Small molecules are favored over polymer systems in many applications due to their ease of synthesis, structural fine-tuning and use in fabrication processes involving vapor deposition.[5] Owing to their controllable and precise electronic properties (e.g. band gap) and easement of blending in polymeric matrix systems, small molecules are excellent candidates as dopant emissive materials in optoelectronic devices.[5]

Among the commonly encountered low molecular-weight fluorescent units, 1,8-napthalimides (NPIs) have secured their position as a versatile class of luminogens owing to their potential applications in biological imaging,[6] fluorescent recognition,[7] optoelectronic materials[8] and as DNA-targeting anticancer agents.[9] However, NPI based solid-state emissive compounds are scarcely reported in literature. In general, NPI based molecules possess strong tendencies to form intermolecular π-π stacking interactions and strong ICT (intramolecular charge transfer) features which can diminish emission yields in their condensed states.[3, 10, 11] In last few years, Reger et al have elegantly utilized such tendencies to design NPI based metal-organic frameworks where NPIs can act as a π-stacking synthons.[11] Such π-π connected compounds can be regarded as suitable candidates for optoelectrnic and semiconductor applications. Although NPIs have been well-studied in coordination complexes and ionic salts, the true

potential of NPI based purely organic molecules have not been explored to any considerable extent.[7-11]

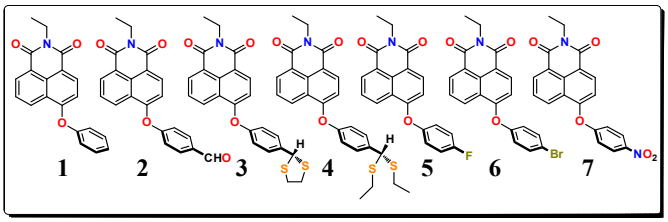

Scheme 1: Structural formulae of compounds **1-7**.

In recent times, apart from the synthetic strategies to prepare sterically encumbered fluorophores, a number of systematic covalent and non-covalent approaches have been developed in order to fine-tune condensed state luminescence in different materials.[12] For instance, the concepts of aggregation-induced emission,[13] crystallization-induced emission enhancement,[14] piezochromism,[15] cocrystals[16] and doping[17] have been inseparably useful to construct newer functional materials. Apart from these efforts, our group has recently demonstrated that systematic synthetic structural perturbations can be also effectively utilized to control the emissive features of organic dyes with or without perturbing their electronic environments.[18] Systematic changes in molecular structure in a series of molecules can serve as an effective method for identifying and controlling different molecular and cumulative properties; interactions etc. and thus serve as a controlling tool at molecular level.

In very recent examples, we have demonstrated the utilizations of such strategies in controlling the solution-state and aggregate-state emission features of NPI based luminogens and fluorescent-conjugates without disturbing their electronic signature at molecular level.[19] The inspiring AIEE (aggregation-induced emission enhancement) features of the compounds have led us to investigate the solid-state emission features of such small molecular and aggregation-prone systems. In this report, we present a series of seven NPIs and present their comparative luminescence properties in solution and solid-state. The systematic investigations of the compounds unveiled a number of intriguing outcomes and provide an insight into the origin of such behaviors. A goal of this project is to understand and fine-tune solid-state luminescence of such small molecular NPI based systems for achieving efficient solid-state emission in these potential but unexplored compounds.

Results and Discussions:

In this study, we present a set of seven (**1-7**) angular and "V" shaped aryloxy substituted NPI molecules. Due to the presence of the oxoaryl moiety, with a bond angle (∠C-O-C) of ~120°, the molecules adopt "V" shaped geometry. Also, due to the steric incapability of the NPI and the oxoaryl moiety to reside in the same plane, the compounds adopt twisted angular structures. These expectations are unambiguously confirmed from their DFT optimized as well as X-ray obtained molecular structures. Compounds **1-4** are known from our previous report[19a] whereas compound **5-7** were newly synthesized and characterized. The aryloxy substituents at the C4-position of the NPI systems are chosen for their lower ICT characteristics compared to C4-amino substituted NPIs. The oxyether bonds also help the molecules to attend an angular "V" shaped geometry which is effective in modulation of the solid-state structures of the NPIs.

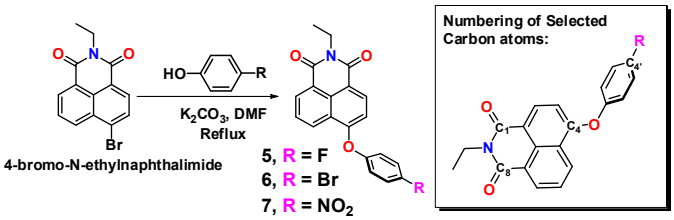

Scheme 2: General synthetic scheme for preparation of **5-7** (left). Numbering in NPIs (right).

Synthesis and Characterizations:

The general synthetic protocol for facile preparation of compounds **1-7** is shown in Scheme 2. Compounds **1-7** were obtained from 4-bromo-N-ethylnaphthalimide with subsequent base assisted nucleophilic phenoxide substitution reaction following purification using column chromatography. The newly prepared compound **5-7** were characterized using ^{1}H NMR, ^{13}C NMR and ESI-Mass. The presence of ^{19}F atoms in compound **5** was also confirmed using ^{19}F NMR. Further, all the compounds (**5-7**) were structurally confirmed from their single-crystals' X-ray diffraction analysis (Figure 1). Thus, among the seven NPIs, single-crystal X-ray structures of six of them (except for **3**) are available for comparative discussions. Except for compound **7** with C4'-nitro substitution, the electronic environments of compound **1-6** are expected to be near similar. However, the flexibilities and the steric bulk of the C4'-substituents of the NPIs are expected to alter their rigidity at molecular level as well as the extents of possible intermolecular interactions.

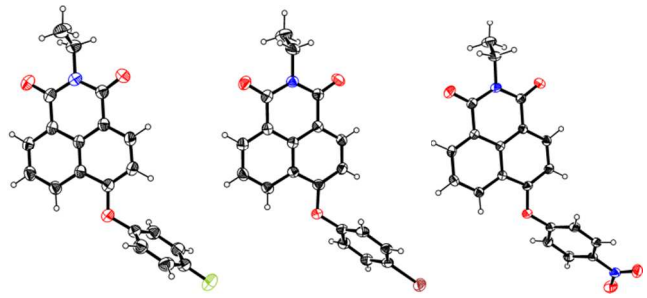

Figure 1: ORTEP diagram of compounds **5-7** respectively (left to right) and obtained from single-crystal X-ray diffraction (C = black, O = red, N = blue, F = green, Br = brown and H = hollow sphere).

Solution-state photophysical properties:

The absorption and emission spectra of the compounds are depicted in Figure 2 and the important photophysical features are tabulated in Table 1. For all the compounds **1-7**, the typical NPI centered absorption bands are observed ~350-360 nm. For compound 2, an enhancement of the band ~275-300 nm is also noticeable which presumably arise due to the presence of an aromatic formyl group. In compound **7**, due to the presence of nitro substituents, a rather broad absorption feature is observed ~250-300 nm. The absorption extinction coefficients of

compounds **1-7** are nearly similar which demonstrate the electronic similarity of the NPIs. In summary, it can be noted that the pendant substituents at the C4'-position do not significantly affect the electronic signature of the NPI moieties. Interestingly, unlike the absorption behavior, the emissive features of compound **1-7** are deeply affected by the C4'-susbtituents. The compounds **1-7** show emission bands of similar spectral shapes ~425 nm which is the NPI dominated cantered emission. However, the emission intensities of the NPIs are remarkably different. Without any substituent, compound **1** shows the highest emission quantum yields of 95.7% in solution state. The addition of fluorine or bromine substituents at the C4'-position lowers the quantum yield of the systems to only limited extent. Addition of –CHO group in compound **3** lowers the emission yields ~43.2%, as the pendant aldehyde group does not participate in its fluorescence (as the NPI core is responsible for the emission) and can only contribute to the non-radiative relaxation pathways. It is well known that more flexible molecular systems, upon excitation, undergo significant structural reorganization in the electronically excited state which facilitates non-radiative relaxation pathways, thereby resulting in low fluorescence quantum yields. The emission yields of compound **3** and **4** are significantly low with respect to the former compounds due to the presence of flexible thioacetal substituents. The lower emission efficiency of compound **4** with respect to compound **3** can be further correlated to the availability of flexible alkyl substituents. Having a pendant electronically active nitro substitution, compound **7** is the least efficient emitter in its solution state. As observed with the previously reported "V" shaped NPIs, compound **5-7** also show considerably intense emission profiles in their aggregated states in THF-Water (1:9) mixtures which can be attributed to their diminished flexibilities in close-packed aggregated states (see the Supporting Information). This behavior also stems the possibilities of achieving solid-state emission of such compounds in solid-states.

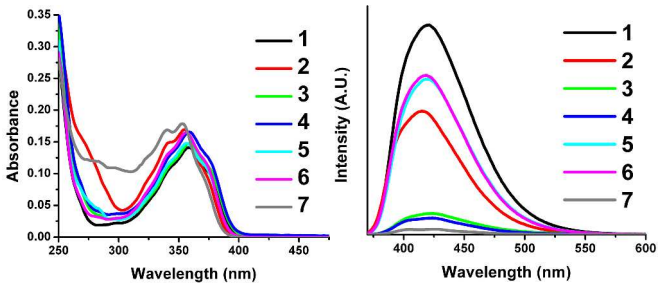

Figure 2: UV-Vis absorption spectra (left) and solution-state emission spectra (right) of compounds **1-7**. (λ_{ex} = 350 nm, 10 μM solutions in THF)

Table 1: Photophysical Properties of **1-7**

	λ_{abs}(nm) (ε, $M^{-1}cm^{-1}$)	TD-DFT obtained HOMO-LUMO transition	λ_{em}(nm) in THF (10 μM)	λ_{em}(nm) in powder state	Stokes' shift $\Delta\lambda$/nm	Φ_F (%) (Solution)	Φ_F (%) (Solid)
1	360 (~14100)	348.12 nm	~420	~440, ~470	~60	95.7	11.1
2	275 (~14220), 355 (~16880)	356.63 nm	~415	~480	~60	43.2	25.8
3	360 (~14750)	348.33nm	~425	~500	~65	9.2	32.1
4	360 (~16600)	348.87 nm	~425	~440, ~470	~65	6.2	35.2
5	360 (~14850)	346.56 nm	~420	~475	~60	73.2	43.5
6	360 (~16450)	346.07 nm	~420	~455	~60	69.0	46.5
7	355 (~17600), 300 (~11000)	364.57 nm	~415	~445, ~470	~60	2.0	1.5

All the given data are for 10μM THF solutions. Quantum yields were calculated using Quinine Sulphate (0.1 M H_2SO_4, λ_{ex} = 350 nm, Φ_F = 57.7 %) solution as reference (represented by R) and using the following formula, $\Phi = \Phi_F \times I \div I_R \times A_R \div A \times \eta^2 \div \eta_R^2$. Where Φ = Quantum Yield, I = Intensity of emission, A = absorbance at λ_{ex}, η = Refractive Index of Solvent.

Solid-state emission properties:

The emission of the compounds (**1-7**) in their aggregated states encouraged us to investigate their emission properties in condensed states. As tabulated in Table 1, compounds **1-6** are moderately emissive in their solid powder states whereas compound **7** is nearly non-emissive in its solid-state. The lower quantum yields of the NPIs (**1**, **2**, **5**, **6** and **7**) in their solid-states compared to the solution state may be attributed to the coupling of electronic states between neighboring molecules (via intermolecular interactions e.g. π-π interactions and O···H interactions) facilitating non-radiative relaxation pathways which is a general observation for solid-state emissive materials. However, this trend find exception in **3** and **4** due to their flexible molecular structures which results in low emission yields in their solution-state but are ineffective in their solid-states.[19a] As shown in Figure 3 and Figure 4, in their solid-state, the NPIs show moderate (~25 nm) to strong red-shift (~65 nm) in their solid-state compared to their THF solutions. The fluorescence intensities of the solution-state and solid-state are presented as normalized spectra in order for the convenient comparison of the two. Such red-shift can be attributed to the solid-state close pack intermolecular interactions which help to form a band-structure in solid-state and lower the effective cumulative band gap in the condensed states of organic luminogens (see DFT computation studies and Figure 13 as discussed *vide-infra*). As shown vide infra, these interactions in compounds **1-7** are mostly π-π stacking interactions. Among all the NPIs, compounds **2** and **3** show comparatively greater red-shift (~60 nm and ~70 nm) of emission in their solid-state with significant lowering of their monomeric emission bands at ~425 nm. Such behaviors can be attributed to strong intermolecular

interactions in solid-state which are evident from the solid-state structure of compound **2** (see later). Although the solid-state structure of compound **3** remained unexplored, the observations of all the other NPIs strongly indicate towards the presence of considerable π-π interactions in its solid-state. Among all the NPIs, compound **6** shows minimum red-shift in its solid-state emission (~30 nm) with respect to pure THF solutions. Also, the emission profile of compound **1** and **6** are relatively sharp with respect to their molecular siblings (**2-5** and **7**). Such behaviors in these compounds (**1** and **6**) suggest towards minimum interactions in their solid-state which can be also correlated to their solid-state structures.

Such red-shifts in emission peaks in the solid-states heavily affect the visual appearance of the compounds (**1-7**) in their solid-state. Due to the complex emission profiles of the NPIs covering ~400-650 nm, compounds **1-3** show greenish luminescence in their solid-state. The considerable contribution of color ~400-450 nm, compound **4**, **5** and **7** appear as bluish-green solids. In contrast, with its sharp emission profile spanning ~455 nm, compound **6** shows blue color luminescence in its solid-state.

Compounds **1-7** also show a vast range of solid-state luminescence quantum yields. Whereas compound **7** can be considered as a very poor emitter in solid-state, compound **1** and **2** are moderately strong emitters. Surprisingly, unlike the solution state, compound **3-6** show strong emission yields in their solid-state which can be attributed to the diminished intermolecular interactions in their solid-state (compared to **1**, **2** and **7**) due to the presence of thioacetyl and halogen substituents. These surprisingly interesting observations led us to hold our conclusions without further investigating the solid-state structural patterns of the compounds.

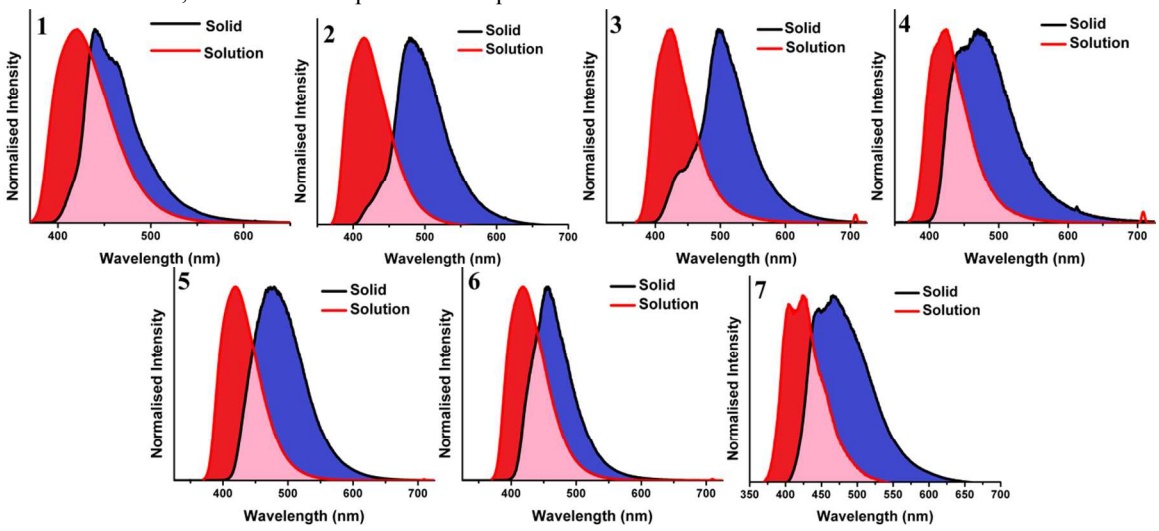

Figure 3: Solid-state emission spectra of compound **1-7** (λ_{ex} = 350 nm) compared to their solution-state (λ_{ex} = 350 nm, 10μM THF solutions) emissions.

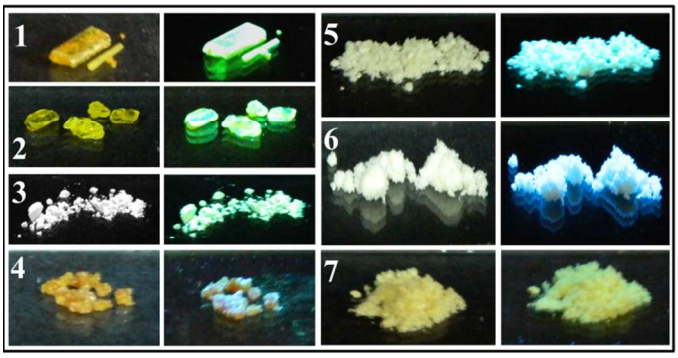

Figure 4: Digital photographs of the compounds **1-7** under white-light illumination and UV-light (254 nm) illumination (left to right respectively).

X-ray Crystal Structures:

Single crystals of all the NPIs (except **3**) were grown via slow evaporation of their DCM solutions. The single crystal structures of compounds **1**, **2** and **4** are reported elsewhere[19a, 19c] and only recalled for a comparative understanding of the series of molecules (**1-7**). The details of the data collection and refinement for compounds **5-7** are given in Table 2.

The structures do not show any level of disorder or solvent inclusion which makes them ideal for a comprehensive assessment of solid-state emission features. Interestingly, compound **1**, **2** and **5-7** crystallized in monoclinic $P2_1/c$ space-group whereas only compound **4** was found to crystallize in a triclinic P_{-1} space-group due to the presence of bulky alkyl substituents. The solid-state structures of the NPIs show dimeric π-π stacking interactions between the two neighboring molecules arranged in antiparallel fashion. As shown in Figure 5, the superimposed transparent space-fill models clearly indicate contact of the neighboring NPI units in compound **1**. Similar observations are also followed in all the other NPIs. Further identification of the close pack intermolecular interactions were also performed in order to understand the cumulative tendencies and van der Waals contacts of the NPIs in their solid-state.

The short-contacts (i.e. distances between atoms in neighboring molecules where the distances between two atoms are shorter than their van der Waals radii) in the crystal structures were unambiguously identified by Hirsfeld surface analysis methods as incorporated in the *CrystalExplorer3.1* software package.[20]

The normalized distance parameter, d_{norm}, represents the parameterized distances between the neighboring atoms where the short-contacts are demonstrated as red spots (distances less than sum of van der Waals radii) through white to blue (distances longer than sum of van der Waals radii).[20d] The Hirsfeld surfaces (and Fingerprint plots) of the molecules in their solid-states are depicted in Figure 6 and the Supporting Information (Figure S9-S20) respectively. As evident from the analysis of Fingerprint plots, the intermolecular interactions in the compounds are dominated by O···H interactions apart from the previously discussed π-π stacking interactions (Table 3 and the Supporting Information). For instance, the O···H interactions in compound **1** covers ~16.1% of all surface contacts which is considerably significant in controlling the packing pattern of the molecules. Similarly, O···H interactions cover nearly 12.4%, 16.8% and 16.7% of the surface contacts in **4**, **5** and **6** respectively. In compounds **2** and **7**, the oxygen atoms of the –CHO and $–NO_2$ groups participate actively in governing close contact O···H interactions and contribute near 24.2% and 34.0% respectively to the all surface contacts. Interestingly, the F and Br atoms in compound **5** and **6** remain practically inactive in forming any short-contact interactions as shown by their Hirsfeld surfaces (Supporting Information). In compound **4**, the interactions between neighboring molecules are mostly dominated by S···H interactions with a significant contribution of 7.3% towards all contacts. These short contacts result in the formation of sheet-like structural patterns of compound **4** in its solid-state (discussed later). As depicted in Figure 6, these short contacts (represented by red-spots in the Hirsfeld Surface) facilitate π-π interactions and other intermolecular interactions in the solid-state. The detailed descriptions of the structures of the NPIs are given in the following section.

The solid-state dihedral arrangements between the 1,8-naphthalimide moiety and the oxoaryl substituents greatly depend on the C4'-substituent and also varies with the nature of crystal packing (see the Supporting Information). Compound **1** and **5** show a dihedral angle of ~83° even though their packing patterns are significantly different. Interestingly, compound **6** shows a dihedral arrangement of only ~70.4° but similar packing arrangements as compound **5**. The diminished dihedral angle can be attributed to the bulky size of the bromine atoms which forces the oxoaryl moieties for compact arrangement to avail space. Similar dihedral arrangement can be also observed in compound **2** (70.3°) which can be also attributed to the special packing arrangement. Interestingly, the lowest dihedral angles (~61°) are observed in compound **4** and **7** due to two completely different reasons. In case of compound **4**, the reason can be attributed to the bulky thioacetyl substituents which forces bending of the oxoaryl moieties in order to provide space. Also the C-S···H-C weak interactions are possibly another driving force for such dihedral arrangements (see the Supporting Information). However, in case of compound **7**, no such forces in act and the diminished dihedral arrangement can be only ascribed to the electronic conjugation acting between the 1,8-naphthalimide moiety and the nitro substituted oxoaryl group. DFT computational studies further support our assumption (see the Supporting Information for the FMOs of the NPIs). The similarity of the dihedral arrangements of compounds **4** and **7** are also reflected on their solid-state spectral shapes. As the molecular geometries and the intermolecular π-π stacking interactions are the common features in these two compounds, the shapes of their emission profiles also appear comparable with each other (Figure 3). However, due the presence of nitro functional groups and extended strong intermolecular contacts with respect to compound **4**, NPI **7** shows rather low quantum efficiency in its solid-state luminescence.

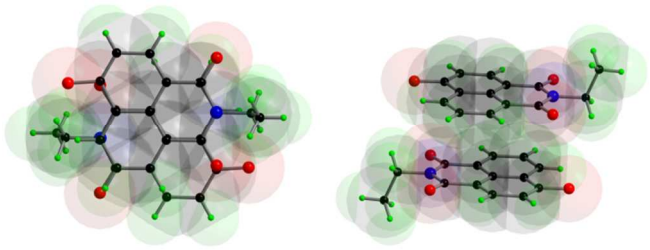

Figure 5: Top-view and side-view (left to right respectively) of the dimeric π-π stacking unit as observed in compound **1**. (Only the NPI units are shown for convenience). The superimposition of a transparent space-fill model is used for the convenience of the visualisation of intermolecular contacts. (Colour code: C = Black, H = Light Green, O = Red, N = Blue)

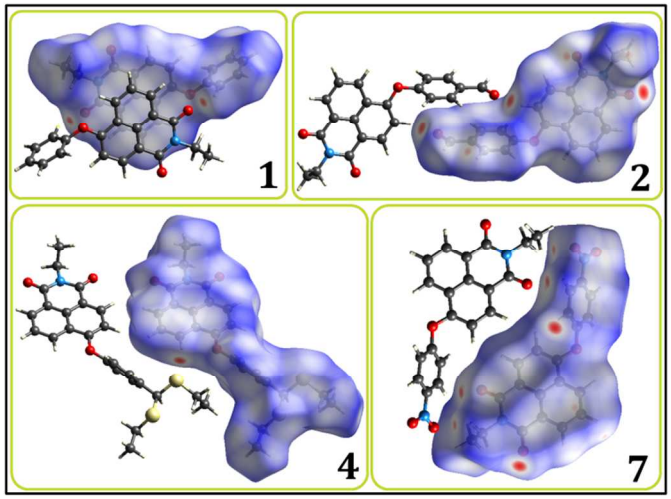

Figure 6: Views of the Hirshfeld surface for compounds **1**, **2**, **4** and **7** where the van der Waals short-contacts are shown by red spots on the surface. The figures depict intermolecular O···H interactions assisted NPI-NPI or aryl-aryl stacking interactions (π-π) interactions in **1** and **2**. In **4**, the S···H short contact interactions are associated with the formation of sheet like arrangements in it solid-state. In compound **7**, considerable greater number of O···H interactions are observed between neighbouring molecules.

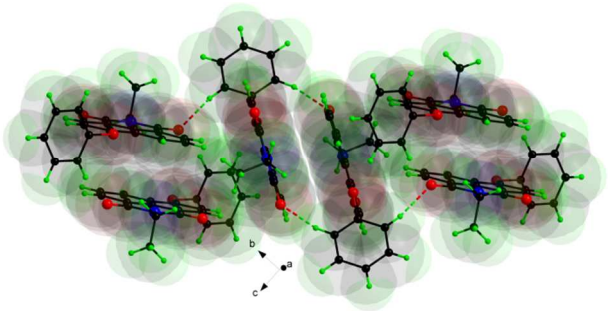

Figure 7: Solid-state packing diagram of compound **1** showing dimeric π-π stacking interactions associated with the intermolecular O···H interactions. The superimposition of a transparent space-fill model is used for the

convenience of the visualisation of intermolecular contacts. (Colour code: C = Black, H = Light Green, O = Red, N = Blue)

The main differences in the structural features of the NPIs arise from the arrangements of the dimeric π-π stacking motifs in their extended forms. As shown in Figure 7-12, the compounds form four distinctly different packing patterns. Surprisingly, compound **1** and **7** share similar kinds packing arrangements which involve orthogonal arrangements of the dimeric π-stacks (Figure 7 and 12 respectively). However, compound **7**, in its extended structures, experience significantly large number of short contacts resulting from O···H interactions which is facilitated by the electron withdrawing nature of the nitro functionality and serve to diminish the fluorescence efficiency of compound **7** (Figure 9 and 10). The two halogen substituted NPIs i.e. compound **5** and **6** form similar structural patterns involving column like arrangements of the stacking units (Figure 11). In these two systems, the NPI-NPI interactions segregate the terminal halogen atoms and the overall arrangement appears as a column like arrangement with two covered with two periodic linear arrangements of halogen atoms (i.e. fluorine and bromine). Compound **2** forms a unique kind arrangement of column like π-π stacking planes with alternate dimeric stacks made of 1,8-naphthalimide motifs (i.e. NPI-NPI stacks) and oxoaryl motifs (i.e. Aryl-Aryl stacks as shown in Figure 8). Although compound **3** was not characterized using single-crystal X-ray diffraction, the observations of the other NPIs helps to anticipate the presence of π-π interactions involving NPI units in its solid-state.

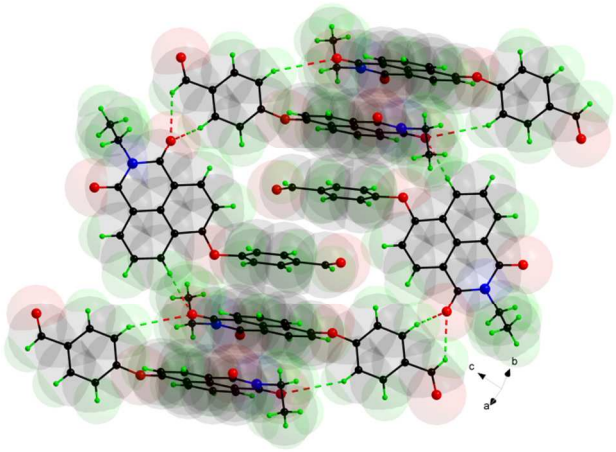

Figure 8: Solid-state packing diagram of compound **2** showing C-H···O-C interactions and column like arrangements of the dimeric alternate stacking units composed of NPI units and aryl rings. The superimposition of a transparent space-fill model is used for the convenience of the visualisation of intermolecular contacts. (Colour code: C = Black, H = Light Green, O = Red, N = Blue)

A uniquely different structural arrangement is observed in case of compound **4**. In solid-state, the π-π stacking interactions of the neighboring 1,8-naphthalimide units form dimeric stacks but the bulky thioalkyl substituents prevent the pendant aryl units in forming any such stacking interactions. The alkyl-alkyl non-polar interactions and the NPI-NPI stacking interactions result in the segregation of the 1,8-naphthalimide units and the thioalkyl units in its solid-state structure. Most interestingly, the dimeric π-π stacking motifs arrange laterally resulting in sheet like structures. Such layered structure in NPI based systems have not been reported hitherto in either molecular systems, ionic salts or in coordination complexes. The precise segregation of the NPI units results in an ordered parallel arrangement of π-surfaces which may be important in light of optoelectronic applications.

In all the solid-state structures, irrespective of their space-group, substituents and overall packing arrangements, the dimeric π-π stacking (NPI-NPI) units of head-to-arrangements involving neighboring 1,8-naphthalimide planes can be observed. The strongest π-π stacking interactions are observed for compound **1** ($d_{\pi-\pi}$ = 3.46 Å, slip angle = 82.0°) and **2** ($d_{\pi-\pi}$ = 3.46 Å, slip angle = 77.5°). In case of compound **3** ($d_{\pi-\pi}$ = 3.60 Å, slip angle = 82.2°), **4** ($d_{\pi-\pi}$ = 3.60 Å, slip angle = 87.0°) and **5** ($d_{\pi-\pi}$ = 3.60 Å, slip angle = 82.9°); the larger π-π distances can be ascribed to the C4'-substituents' bulk and inefficient participation in any strong intermolecular interactions (unlike the –CHO and $–NO_2$ groups). In compound **7** ($d_{\pi-\pi}$ = 3.54 Å, slip angle = 73.3°), due to strong participation of $–NO_2$ substituents in other supramolecular interactions, the effective π-π interactions are weakened compared to **1** and **2** forms a slipped arrangement rather than a direct overlapping arrangement.

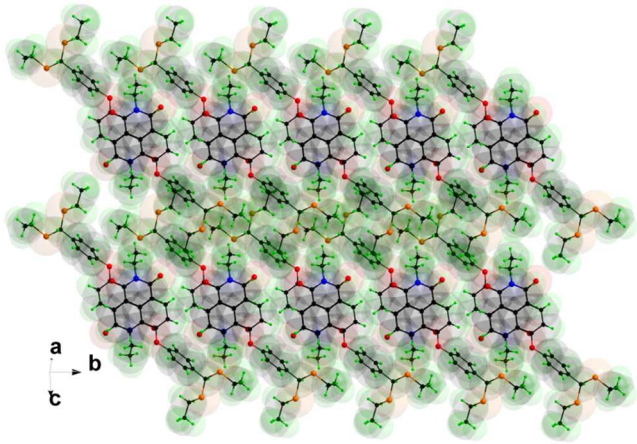

Figure 9: Solid-state packing diagram of compound **4** showing sheet-like structure arising from the separation of the thioalkyl units and the aromatic π-π stacking units. The superimposition of a transparent space-fill model is used for the convenience of the visualisation of intermolecular contacts. (Colour code: C = Black, H = Light Green, O = Red, N = Blue, S = Orange)

The solid-state structural arrangements also provide to be useful to understand the solid-state emission profiles and efficiencies of compound **1-7**. As discussed earlier, the red-shift in the emission spectra of the compounds in their solid-states compared to the solution states can be well attributed to the formation of dimeric π-π stacking units. In addition to this effect, Ar-Ar stacking interactions and availability of EWGs (electron withdrawing groups) in compound **2** and **7** result in the formation of other interactions (i.e. O···H interactions etc.) result in a rather higher red-shifted broad emission profiles in these two compounds. Comparatively, compounds **5** and **6** show relatively sharper and less red-shifted emission bands which can be attributed to their weaker NPI-NPI stacking interactions. The broad emission spectral shape of compound **4** in its solid-state is indicating towards to the electronic coupling interactions between the neighboring stacking units.

Table 2. Crystallographic data and refinement parameters for **5-7.**

	5	**6**	**7**
Empirical formula	$C_{20}H_{14}FNO_3$	$C_{20}H_{14}BrNO_3$	$C_{20}H_{14}N_2O_5$
FW	335.32	396.23	362.33
T (K)	293(2) K	293(2) K	293(2) K
crystal system	Monoclinic	Monoclinic	Monoclinic
space group	$P\,2_1/c$	$P\,2_1/c$	$P\,2_1/c$
a/Å	8.972(3)	9.008(7)	13.916(5)
b/Å	7.295(3)	7.848(6)	11.329(4)
c/Å	24.757(10)	24.086(19)	10.530(4)
α/deg	90	90	90
β/deg	96.905(7)	100.229(13)	98.067(7)
γ/deg	90	90	90
V/Å^3	1608.8(11)	1676(2)	1643.6(10)
Z	4	4	4
ρ_{calcd} (g cm^{-3})	1.384	1.571	1.464
μ (Mo Kα) (mm^{-1})	0.101	2.472	0.107
λ/Å	0.71073	0.71073	0.71073
F (000)	696	800	752
collected reflns	17298	14934	18121
unique reflns	3789	3736	3924
GOF (F^2)	1.113	0.954	1.046
R_1[I>2σ(I)][a]	0.0588	0.0652	0.0579
wR_2[I>2σ(I)][b]	0.1392	0.1558	0.1161

[a]$R_1 = \Sigma \big| \, |F_o| - |F_c| \, \big| / \Sigma |F_o|$. [b]$wR_2 = [\Sigma\{w(F_o^2 - F_c^2)^2\}/\Sigma\{w(F_o^2)^2\}]^{1/2}$

Table 3. Important bond lengths and bond angles involved in supramolecular architectures of compounds **1, 2** and **4-7**.

Compound	**Intermolecular interactions**	(Å)	(°)
1	C12-O2•••H20-C20 C12-O2•••H16-C16	2.571 2.597	152.49 157.27
2	C12-O2•••H5-C5 C21-O4•••H3-C3 C11-O1•••H19-C19 C11-O1•••H19-C19	2.436 2.495 2.586 2.705	157.01 162.17 129.27 128.47
4	C21-S1•••H5-C5	2.839	163.92
5	C12-O2•••H16-C16 C12-O2•••H20-C20 C11-O1•••H17-C17 C11-O1•••H19-C19	2.492 2.401 2.502 2.452	158.16 163.73 119.90 132.34
6	C12-O2•••H16-C16 C12-O2•••H20-C20 C11-O1•••H17-C17 C11-O1•••H19-C19	2.558 2.563 2.528 2.544	173.17 168.87 139.96 133.50
7	N2-O4•••H17-C17 C11-O1•••H19-C19 C12-O2•••H20-C20	2.631 2.520 2.520	147.75 127.49 167.42

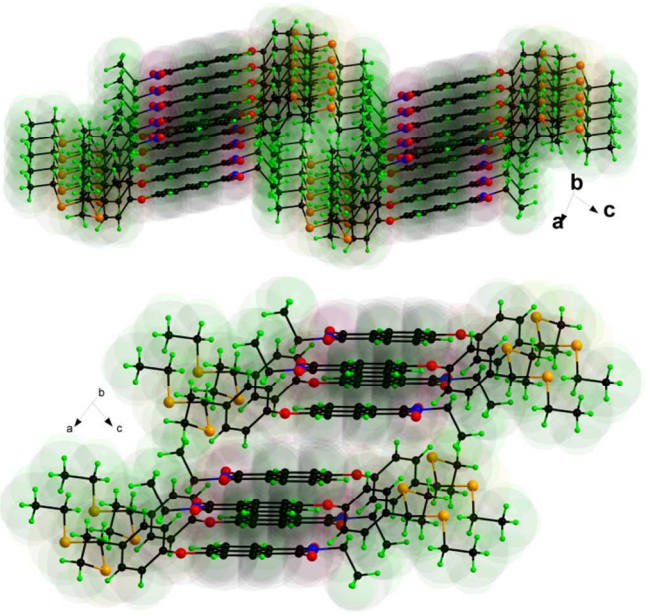

Figure 10: Side view of a single-layer (top) and two proximal layers (bottom) of compound **4**. The superimposition of a transparent space-fill model is used for the convenience of the visualisation of intermolecular contacts. (Colour code: C = Black, H = Light Green, O = Red, N = Blue, S = Orange)

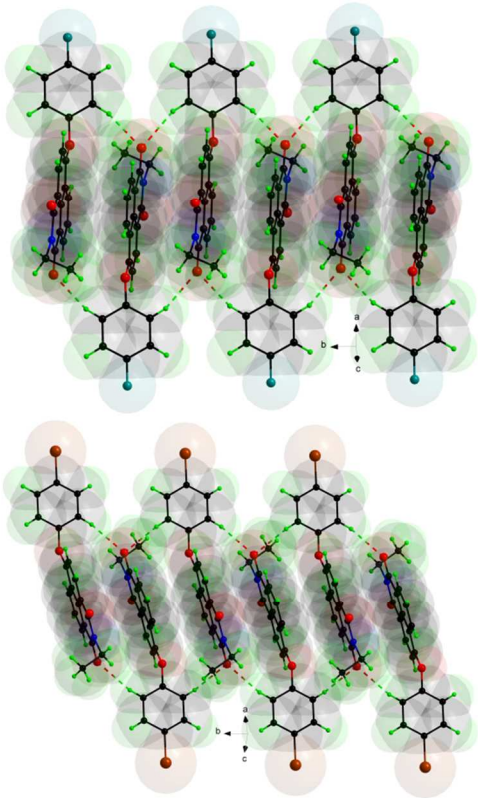

Figure 11: Solid-state packing of compound **5** (top) and **6** (bottom). The superimposition of a transparent space-fill model is used for the convenience of the visualisation of intermolecular contacts. (Colour code: C = Black, H = Light Green, O = Red, N = Blue, F = Dark Green, Br = Brown)

The structural patterns of the compounds also correlate with the observed emission efficiencies of the NPIs in their solid-state. Whereas the strongly interacting systems like compound **1**, **2** and **7** relatively lower quantum yields in solid-state, weakly interacting systems like compound **3-6** are strong emitters in their solid-states. The emission efficiency of compound **3-6** can be attributed to the effective lateral separation of the compounds which result in effective dilution of the fluorophore units in solid-state. For instance, the lateral displacement of the proximal NPI units in compounds **5** and **6** are ~9.0 Å. Whereas in compound **4**, due to absence of any other column like arrangements and strong lateral interactions, the distance is relatively smaller (~8.7 Å). Such apparently small changes in intermolecular interactions often impart significantly large outcome in the bulk properties of solid-state emissive materials.[12] The relative arrangements of the π-π stacking interactions are probably another important aspect of controlling solid-state luminescence efficiency. Whereas parallel arrangements as observed in **4**, **5** and **6** enhance the fluorescence emission yields of the materials, strongly interacting systems with orthogonal arrangements contribute negatively in their solid-state luminescence properties. These observations are in agreement with the previously perceived behaviours of other solid-state organic luminogens.[12]

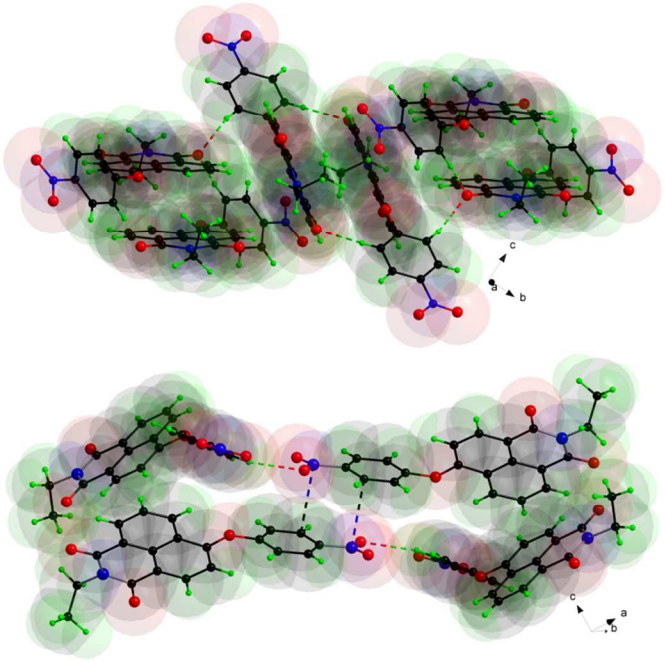

Figure 12: Orthogonal arrangements of dimeric stacked units (top) and other solid-state interactions (bottom) in compound **7**. The superimposition of a transparent space-fill model is used for the convenience of the visualisation of intermolecular contacts. (Colour code: C = Black, H = Light Green, O = Red, N = Blue)

DFT computational studies:

After understanding the solid-state structure of the NPIs, DFT computational studies (B3LYP/6-31G(d)) were performed in order to understand the cumulative and molecular properties of the compounds (see 'DFT Computational Methods' for details). In this regard, gas-phase geometry optimizations of the NPIs were performed. The near similar band-gap (as obtained from DFT and TD-DFT vertical excitation calculations) supports the experimentally observed similar UV-Vis absorption profiles of the compounds (Table 1 and the Supporting Information). TD-DFT obtained 1st excited state structures of the compounds show considerable reorientation of the dihedral arrangement between the NPI and the oxoaryl moiety indicating towards the structural flexibility of the compounds (Supporting Information).[19a]

The ground state and gas phase optimized structures of compound **1-7** resemble closely to the single crystal X-ray obtained structures (see Reference 19a for DFT results of compounds **1-4** and the Supporting Information for compounds **5-7**). The dihedral arrangements of the 1,8-naphthalimide moiety and the aryl substituents were found to be ~87-89° whereas for compound **7**, the same was found to be ~64.8°. As discussed earlier, the lower dihedral arrangement in compound **7** is its molecular property arising from the nitro group assisted conjugation between the NPI unit and the oxoaryl moiety (see Figure S39 in the Supporting Information). Also, in 7, due to this conjugation, emission efficiency also diminishes in the solution state as the effective size and flexibility of the fluorophore becomes comparatively larger with respect to **1-6**. Similar observations can be also followed in the previously discussed crystal structures of the compound. Evidently, the nitroaryl moiety involve in relatively higher conjugation with the 1,8-naphthalimide moiety (compared to **5** and **6**). The FMOs (Frontier Molecular Orbitals) of the compounds **5-7** further support this statement (see the Supporting Information). Whereas for compounds **1-6**, the FMOs are mainly localized on the 1,8-naphthalimide moieties, in compound **7**, significant involvement is also observed from the nitroaryl moiety (see the Supporting Information for the FMOs of **1-7**).

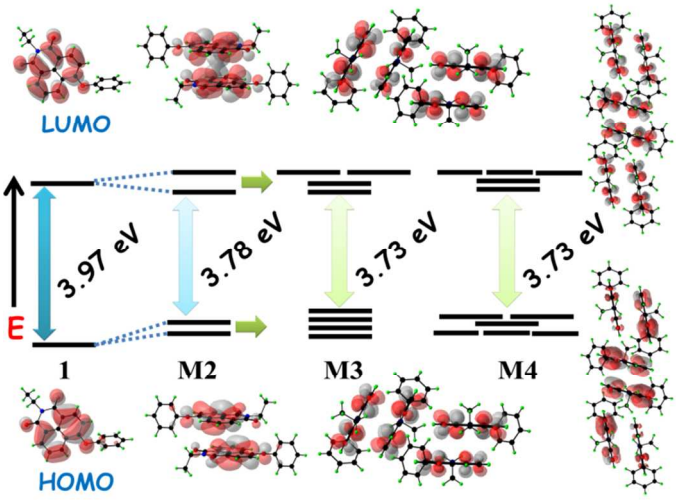

Figure 13: DFT B3LYP/6-31G(d) obtained selected MOs and relative band gaps of the monomeric units of **1** and model systems **M2**, **M3** and **M4** (from left to right respectively). The FMOs are shown in the figure (isovalue = 0.02).

Computational investigations also helped us to understand the cumulative behavior of the compounds **1-7** in their solid-states. The crystal geometries of the dimeric π-stacks and their extended forms were taken into considerations and their absolute energies were calculated using B3LYP/6-31G(d) level of theory. The FMOs of the model structures for compound **1**

are shown in Figure 13. Evidently, on moving from single molecular **1** to its dimeric stack model **M2**, the degeneracy of the FMOs is broken with lowering of HOMO and LUMO energy levels compared to **1**. The effective band gap is also diminished in this process which can explain the red-shifts of the emission spectra of the NPIs in their solid-states. On further going from a dimeric model **M2** to two orthogonally substituted dimeric stacking model system **M3**, the effective band gap further decreases but the rate of decrement becomes slower. Further addition of another dimeric stacking (**M4**) unit does not make any effective change in the overall band gap as degeneracies are also being formed in the near FMO energy levels. However, these simple illustrations effectively demonstrate how the formation of extended networks results in a finite decrement of the effective band gap where the effects are mostly local in nature. The illustration also demonstrates that the close pack molecules tend to form a band structure in solid-state. Thus, electronically excited molecules may also avail relaxation by participation of neighboring molecules, which in turn, is effectively responsible for the lowering of the quantum yield of compound **1** (and also **2**, **5-7**) in solid-state compared to solution-state. However, in **3** and **4**, the flexible alkyl units are responsible for their low emission yields in solution states. This statement is also supported by the previously observed and significantly greater AIEE (aggregation-induced emission enhancement) properties of **3** and **4**.[19a] In solid-state, the structural rigidity of the systems coupled with the precisely ordered parallel arrangements of the molecules result in an effective enhancement of emission efficiencies in their solid-states. This is also reflected in the aggregation-induced emission changes of the compounds which have been described thoroughly in our previous reports.[19a-b]

Comparative Discussion:

The results demonstrated/described in the past sections can be combined and summarised to understand the compounds 1-7 in an ample manner. UV-Vis and emission studies in solution-state showed that compounds **1-7** have almost similar band-gap in their solution states i.e. molecular states which inevitably implies towards the electronic similarity of the compounds' FMOs and the apparent passive effects of the C4'-substituents. The emission yields of the compounds in solution states are controlled by their structural rigidity (i.e. presence of flexible substituents e.g. thioacetyl groups in **3** and **4** lower their emission yields in the solution-state) which can well explain the highest emission yields of compound **1**, **5** and **6** as well as the poor emission yields of 3 and 4. The presence of nitro group in compound **7** also results in quenching of fluorescence. However, this simplicity is not maintained in their solid-state. The red-shift in the emission profiles of compounds **1-7** in their solid-state compared to solution-states is effectively controlled by the solid-state arrangement of the molecules. The higher red-shifts observed in **2**, **7** and the sharp and least shifted blue emission bands in compound 6 supported these assumptions. The apparently irrelevant and passive substituents also greatly control the nature of extended structures in solid-forms. Whereas, compound **1** and **7** form orthogonal arrangements of stacking dimers, compound **5** and **6** prefer column like arrangements. In contrast, compound **2** forms a rather heavily stacked and H-bonded solid-state structure. Having bulky non-polar alkyl groups, compound **4** form segregation of the aromatic and alkyl moieties in its solid-state resulting in layer like extended networks. The emission colour and yields of the compounds are well-correlated tot the solid-state structures of the NPIs. In addition, DFT computational investigations also helped to understand the molecular and cumulative properties of the NPIs. Whereas, the studies confirmed the similar band-gap and FMO distribution of the compounds, it also provide useful inferences about the extended structure and its electronic nature. The energy calculations show that the electronic stabilisations of the molecules in their solid-states are localised and convergent while forming extended networks. The study explains how finite red-shift occurs in the solid-state structures of the NPIs.

Experimental Section

Materials and Methods:

4-bromo-N-ethylnaphthalimide was synthesized following known literature procedure.[21] The 400 MHz ^{1}H NMR, 100 MHz ^{13}C NMR, 376 MHz ^{19}F NMR were collected on a Bruker Advance 400 MHz NMR spectrometer. All solution ^{1}H and ^{13}C spectra were referenced internally to the solvent signal. ^{19}F NMR spectra was referenced externally to $BF_3.Et_2O$ ($\delta = 0$) in C_6D_6. Electronic absorption spectra were collected on a Perkin Elmer LAMBDA 750 UV/visible spectrophotometer. Electrospray ionization mass spectral measurements were done using Esquire 3000 plus ESI (Bruker Daltonics) and Q-TOF Mass spectrometers. Due to poor solubility of compounds **5-7** in MeOH, Acetonitrile and poor ionizations of the compunds, trifluoroacetic-acid was used as an external agent. Solutions were prepared using a microbalance (± 0.1mg) and volumetric glassware and then charged in quartz cuvettes. Fluorescence emission studies were carried out on a Horiba JOBIN YVON Fluoromax-4 spectrometer. Absolute quantum yields were measured using quanta-phi integrated sphere module equipped in a Fluoromax-4 spectrophotometer. Single-crystal X-ray diffraction data were collected with a Bruker D-QUEST diffractometer. The data were integrated using SAINT, and an empirical absorption correction was applied with SADABS.[22] The structures were determined by direct methods using SHELXS-97 and refined by full-matrix least-squares techniques against F_o^2 using SHELXL-97. All the non-hydrogen atoms were refined with anisotropic displacement parameters, while the hydrogen atoms were refined isotropically on the positions calculated using a riding model. TEM images were collected from a JEOL field emission Transmission-Electron-Microscope JEM-2100F under 80KV working voltage.

DFT computational Methods:

The hybrid B3LYP[23] functional has been used in all calculations as incorporated in *Gaussian 09* package,[24] mixing the exact Hartree-Fock-type exchange with Becke's exchange functional[25] and that proposed by Lee-Yang-Parr[26] for the correlation contribution. We used 6-31G(d) basis set for all the atoms which provides reasonably high quality results in moderate timescales. All ground state geometry optimizations were monitored by subsequent frequency test to establish stationary points. The model systems **M2-M4** were created using crystallographic coordinates and used for single-point energy calculations without any further optimizations. 1st excited state optimizations for compound **1-7** were also performed (starting from ground state optimized geometries) using TD-DFT (B3LYP/6-31G(d)) method.

General Synthetic Procedures:

In a solution of 4-bromo-N-ethylnaphthalimide (304 mg, 1 mmol) in DMF (20 ml), substituted-phenol (1.5 mmol; *p*-fluorophenol for **5**, *p*-bromophenol for **6** and *p*-nitrophenol for **7**) and of K_2CO_3 (500 mg) were added and the mixture was heated to reflux for 24 hours. The solvent was evaporated under vacuum and the residue was extracted using EtOAc (100 ml). The organic layer was washed with H_2O for several times followed by washing with saturated NaCl solution. The organic layer was dried over anhydrous Na_2SO_4 and the solvent was removed under reduced pressure to get crude product, which was further purified using column chromatography (Dichloromethane as eluent).

Characterizations Data:

Compound **5:**

Yield: 205 mg (61%).^{1}H NMR (400 MHz, $CDCl_3$, δ ppm) 1.33 (t, J = 8.0 Hz, 3H), 4.24 (q, J = 8.0 Hz, 2H), 6.86 (d, J = 8.0 Hz, 1H), 7.17 (m, 4H), 7.78 (t, J = 8.0 Hz, 1H), 8.45 (d, J = 8.0 Hz, 1H), 8.66 (m, 2H). ^{13}C NMR (100.00 MHz, $CDCl_3$, δ ppm) 164.7, 164.0, 160.4, 151.0, 133.2, 132.4, 130.1, 128.9, 127.0, 124.2, 123.2, 122.9, 117.7, 117.5, 117.2, 110.5, 35.9, 13.9. ^{19}F NMR (376.00 MHz, CDCl3, δ ppm) -116.6. HRMS (Q-TOF): Mcalc.($C_{20}H_{14}FNO_3H$) = 336.1031 Da; found: 336.1036 Da [M+H]+.

Compound **6:**

Yield: 250 mg (63%).^{1}H NMR (400 MHz, $CDCl_3$, δ ppm) 1.33 (t, *J* = 8.0 Hz, 3H), 4.24 (q, *J* = 8.0 Hz, 2H), 6.93 (d, *J* = 8.0 Hz, 1H), 7.07 (d, *J* = 8.0 Hz, 2H), 7.59 (d, *J* = 8.0 Hz, 2H), 7.79 (t, *J* = 8.0 Hz, 1H), 8.47 (d, *J* = 8.0 Hz, 1H), 8.64 (m, 2H). ^{13}C NMR (100.00 MHz, $CDCl_3$, δ ppm) 164.6, 164.0, 159.7, 154.6, 134.0, 133.1, 132.9, 130.1, 128.8, 127.2, 124.4, 123.2, 122.9, 118.9, 117.6, 111.3, 35.9, 13.9. HRMS (Q-TOF): Mcalc.($C_{20}H_{14}BrNO_3H$) = 396.0235 (100%) and 398.0215 (100%) Da; found: 396.0224 (100%) and 398.0205 (100%) Da $[M+H]^+$.

Compound **7:**

Yield: 125 mg (34%).^{1}H NMR (400 MHz, $CDCl_3$, δ ppm) 1.34 (t, *J* = 8.0 Hz, 3H), 4.26 (q, *J* = 8.0 Hz, 2H), 7.25 (m, 3H), 7.80 (t, *J* = 8.0 Hz, 1H), 8.32 (d, *J* = 8.0 Hz, 2H), 8.49 (d, *J* = 8.0 Hz, 1H), 8.55 (d, *J* = 8.0 Hz, 1H), 8.70 (d, *J* = 8.0 Hz, 1H). ^{13}C NMR (100.00 MHz, $CDCl_3$, δ ppm) 163.6, 163.0, 161.0, 156.6, 144.0, 132.0, 131.9, 129.6, 127.7, 127.1, 126.1, 124.3, 122.9, 119.0, 118.9, 114.0, 35.3, 13.1. HRMS (Q-TOF): Mcalc.($C_{20}H_{15}N_2O_5H$) = 363.0981 Da; found: 363.0940 Da $[M+H]^+$.

Conclusions

In conclusions, investigations of a series of structurally close NPIs (**1-7**) demonstrated the significant effects of apparently unrelated substituents in controlling their solution state as well as solid-state properties. The difference of the luminescence properties of the compounds in their solid-state were correlated to their solid-state structures which were further supported by DFT investigations. The NPIs form a vast range of extended packing structures (i.e. columns, sheet-layers, orthogonal arrangements etc.) depending on the electronic and steric demands of the C4'-substituents. The studies led us to conclude how small alterations can be used to fine-tune molecular environment and intermolecular interactions at the molecular level. The structural, DFT computational and crystallographic analyses provide a strong correlation to the experimentally observed photophysical properties of the NPIs. It is demonstrated that isolation of the fluorescent units without altering the nature of intermolecular forces (e.g. **5** and **6**) can result in significant changes in their emission colors as well as luminescent quantum yields. Also, the unique arrangements of fluorophores (e.g. sheet like structure of **4**) can effectively enhance the emission efficiencies of the materials even beyond their solution state properties. Also, structurally comparable systems (e.g. **1** and **4**) with differences only in their close contacts can also show large differences of their emission properties. Evidently, the fine-tuning of solid-state luminescent properties of organic materials are greatly dependent on several correlated and uncorrelated factors and require close attention at each individual entity in order to understand the pattern in a considerable large number of examples. This work is expected to contribute to the enrichment of such understanding.

Acknowledgements

PT thanks IISc for the financial assistance. SM thanks CSIR, New Delhi for the Shyama Prasad Mukherjee fellowship. The authors thank Mr. R. Sathiskumar and Mr. Barun K. Barman for his help. We also thank the anonymous reviewers for their helpful suggestions and comments.

Notes and references

[a] Department of Inorganic & Physical Chemistry, Indian Institute of Science, Bangalore 560 012 (India); Fax: (+91)-8023601552; E-mail: sanjoymkj@ipc.iisc.ernet.in, thilagar@ipc.iisc.ernet.in.

Electronic Supplementary Information (ESI) available: [NMR, extended photophysical studies, DFT computational data, SEM and TEM data and CIF files. CCDC 961304-961306]. See DOI: 10.1039/b000000x/

(1) (a) R. H. Friend, R. W. Gymer, A. B. Holmes, J. H. Burroughes, R. N. Marks, C. Taliani, D. D. C. Bradley, D. A. Dos Santos, J. L. BreÂ das, M. LoÈgdlund and W. R. Salaneck, *Nature*, 1999, **397**, 121. (b) G Kranzelbinder and G Leising, *Rep. Prog. Phys.*, 2000, **63**, 729. (c) A. W. Hains, Z. Liang, M. A. Woodhouse and B. A. Gregg, *Chem. Rev.*, 2010, **110**, 6689. (d) M. Mas-Torrent and C. Rovira, *Chem. Rev.*, 2011, **111**, 4833. (e) C. Wang, H. Dong, W. Hu, Y. Liu and D. Zhu, *Chem. Rev.*, 2012, **112**, 2208.

(2) (a) J. Kalinowski, Organic Light-Emitting Diodes: Principles, Characteristics & Processes, CRC press, 2004. (b) T. Tsujimura, OLED Display Fundamentals and Applications, Wiley, 2012. (c) A. Buckley, Organic Light-Emitting Diodes (OLEDs): Materials, Devices and Applications, Woodhead Publishing, 2013.

(3) J. R. Lakowicz, Principles of Fluorescence Spectroscopy, Springer, Singapore, 2006.

(4) M. Shimizu and T. Hiyama, *Chem.-Asian J.*, 2010, **5**, 1516.

(5) (a) M. Mas-Torrent and C. Rovira, *Chem. Soc. Rev.* 2008, **37**, 827. (b) B. Walker, C. Kim and T.-Q. Nguyen, *Chem. Mater.*, 2011, 23, 470. (c) Y. Lin, Y. Li and X. Zhan, *Chem. Soc. Rev.*, 2012, **41**, 4245. (d) J. Kao, K. Thorkelsson, P. Bai, B. J. Rancatore and T. Xu, *Chem. Soc. Rev.*, 2013, **42**, 2654.

(6) (a) D. Srikun, E. W. Miller, D. W. Domaille, and C. J. Chang, *J. Am. Chem. Soc.*, 2008, **130**, 4596. (b) M. H. Lee, J. H. Han, P.-S. Kwon, S. Bhuniya, J. Y. Kim, J. L. Sessler, C. Kang, and J. S. Kim, *J. Am.*

Chem.Soc., 2012, **134**, 1316. (c) L. Yuan, W. Lin, K. Zheng, L. He and W. Huang, *Chem. Soc. Rev.*, 2013, **42**, 622. (d) C. Zhang, Z. Liu, Y. Li, W. He, X. Gao and Z. Guo, *Chem. Commun.,* 2013, **49**, 11430.

(7) (a) X. Qian, Y. Xiao, Y. Xu, X. Guo, J. Qiana and W. Zhua, *Chem. Commun.*, 2010, **46**, 6418. (b) R. M. Duke, E. B. Veale, F. M. Pfeffer, P. E. Kruger and T. Gunnlaugsson, *Chem. Soc. Rev.,* 2010, **39**, 3936. (c) B. Zhu, X. Zhang, Y. Li, P. Wang, H. Zhang and X. Zhuang, *Chem. Commun.*, 2010, **46**, 5710. (d) Z. Xu, J. Yoon and D. R. Spring, *Chem. Commun.*, 2010, **46**, 2563. (e) L. A. Montoya and M. D. Pluth, *Chem. Commun.*, 2012, **48**, 4767. (f) P. Mahato, S. Saha, E. Suresh, R. D. Liddo, P. P. Parnigotto, M. T. Conconi, M. K. Kesharwani, B. Ganguly and A. Das, *Inorg. Chem.*, 2012, **51**, 1769. (g) M. H. Lee, J. H. Han, J.-H. Lee, H. G. Choi, C. Kang, and J. S. Kim, *J. Am. Chem. Soc.*, 2012, **134**, 17314. (h) C. Yu, X. Li, F. Zeng, F. Zheng and S. Wu, *Chem. Commun.*, 2013, **49**, 403. (i) L. Chen, W. Sun, J. Li, Z. Liu, Z. Ma, W. Zhang, L. Du, W. Xu, H. Fang and M. Li, *Org. Biomol. Chem.*, 2013, **11**, 378. (j) M. Kumar, N. Kumar and V. Bhalla, *Chem. Commun.*, 2013, **49**, 877. (k) Y. Zhou, Y.-W. Yao, Q. Qi, Y. Fang, J.-Y. Lic and C. Yao, *Chem. Commun.*, 2013, **49**, 5924. (l) M. H. Lee, B. Yoon, J. S. Kim and J. L. Sessler, *Chem. Sci.*, 2013, **4**, 4121.

(8) (a) Y. Zhang, W. Zhu, W. Wang, H. Tian, J. Sua and W. Wang, *J. Mater. Chem.*, 2002, **12**, 1294. (b) D. Kolosov, V. Adamovich, P. Djurovich, M. E. Thompson, and C. Adachi, *J. Am. Chem. Soc.*, 2002, **124**, 9945. (c) G. Wang, S. Miao, Q. Zhang, H. Liu, H. Li, N. Li, Q. Xu, J. Lu and L. Wang, *Chem. Commun.,* 2013, **49**, 9470.

(9) (a) I. Ott, Y. Xu, J. Liu, M. Kokoschka, M. Harlos, W. S. Sheldrick and X. Qian, *Bioorg. Med. Chem.*, 2008, **16**, 7107; (b) Q. Yang, P. Yang, X. Qian and L. Tong, *Bioorg. Med. Chem. Lett.*, 2008, **18**, 6210; (c) M. Lv and H. Xu, *Curr. Med. Chem.*, 2009, **16**, 4797; (d) L. Ingrassia, F. Lefranc, R. Kiss and T. Mijatovic, *Curr. Med. Chem.*, 2009, **16**, 1192. (e) Z. Chen, X. Liang, H. Zhang, H. Xie, J. Liu, Y. Xu, W. Zhu, Y. Wang, X. Wang, S. Tan, D. Kuang and X. Qian, *J. Med. Chem.*, 2010, **53**, 2589; (f) S. Banerjee, J. A. Kitchen, T. Gunnlaugsson and J. M. Kelly, *Org. Biomol. Chem.*, 2012, **10**, 3033. (g) S. Banerjee, E. B. Veale, C. M. Phelan, S. A. Murphy, G. M. Tocci, L. J. Gillespie, D. O. Frimannsson, J. M. Kelly and T. Gunnlaugsson, *Chem. Soc. Rev.*, 2013, **42**, 1601. (h) S. Banerjee, J. A. Kitchen, S. A. Bright, J. E. O'Brien, D. C. Williams, J. M. Kelly and T. Gunnlaugsson, *Chem. Commun.*, 2013, **49**, 8522. (i) C. P. Bagowski, Y. You, H. Scheffler, D. H. Vlecken, D. J. Schmitz and I. Ott, *Dalton Trans.*, 2009, 10799. (j) K. J. Kilpin, C. M. Clavel, F. Edafe, and P. J. Dyson, *Organometallics*, 2012, **31**, 7031.

(10) J. Gierschner, L. Lüer, B. Milián-Medina, D. Oelkrug, and H.-J. Egelhaaf, J. Phys. Chem. Lett., 2013, 4, 2686.

(11) (a) D. L. Reger, J. D. Elgin, R. F. Semeniuc, P. J. Pellechia and M. D. Smith, *Chem. Commun.*, 2005, 4068. (b) D. L. Reger, A. Debreczeni, B. Reinecke, V. Rassolov, and M. D. Smith, *Inorg. Chem.*, 2009, **48**, 8911. (c) D. L. Reger, A. Debreczeni, and M. D. Smith, *Inorg. Chem.*, 2012, **51**, 1068.

(12) (a) D. Yan and D. G. Evans, *Mater. Horiz.*, 2014, **1**, 46. (b) S. Varughese, *J. Mater. Chem. C*, 2014, **2**, 3499. (c) S. Mukherjee and P. Thilagar, *Proc. Natl. Acad. Sci., India, Sect. A Phys. Sci.*, 2014, **84**, 131.

(13) (a) J. Luo, Z. Xie, J. W. Y. Lam, L. Cheng, H. Chen, C. Qiu, H. S. Kwok, X. Zhan, Y. Liu, D. Zhu and B. Z. Tang, Chem. Commun., 2001, 1740. (b) Y. Hong, J.W. Y. Lam and B. Z. Tang, *Chem. Commun.*, 2009, 4332. (c) Y. Hong, J. W. Y. Lam and B. Z. Tang, *Chem. Soc. Rev.*, 2011, **40**, 5361.

(14) (a) Y. Dong, J. W. Y. Lam, A. Qin, Z. Li, J. Sun, H. H.-Y. Sung, I. D. Williams and B. Z. Tang, *Chem. Commun*., 2007, 40. (b) Y. Dong, J. W. Y. Lam, A. Qin, J. Sun, J. Liu, Z. Li, J. Sun, H. H. Y. Sung, I. D. Williams, H. S. Kwok and B. Z. Tang, *Chem. Commun.*, 2007, 3255.

(15) Y. Dong, B. Xu, J. Zhang, X. Tan, L. Wang, J. Chen, H. Lu, S. Wen, B. Li, L. Ye, B. Zou and W. Tan, *Angew. Chem. Int. Ed.*, 2011, **51**, 10782.

(16) D. Yan, A. Delori, G. O. Llyod, T. Friscic, G. M. Day, W. Jones, J. Lu, M. Wei, D. G. Evans and X. Duan, *Angew. Chem. Int. Ed.*, 2011, **50**, 12483.

(17) O. Bolton, K. Lee, H.-J. Kim, K. Y. Lin and J. Kim, *Nat. Chem.*, 2011, **3**, 205.

(18) (a) C. A. S. P, S. Mukherjee and P. Thilagar, *Chem. Commun.*, 2013, **49**. 993. (b) C. A. S. P, S. Mukherjee and P. Thilagar, *J. Mater. Chem. C*, 2013, **1**, 4691. (c) P. Sudhakar, S. Mukherjee, and P. Thilagar, *Organometallics*, 2013, **32**, 3129.

(19) (a) S. Mukherjee and P. Thilagar, *Chem. Commun.*, 2013, **49**. 7292. (b) S. Mukherjee and P. Thilagar, *Chem. Eur. J.*, 2014, **20**, 8012-8023. (c) S. Mukherjee and P. Thilagar, *Chem. Eur. J.*, 2014, **20**, 9052-9062.

(20) (a) CrystalExplorer (Version 3.1), S.K. Wolff, D.J. Grimwood, J.J. McKinnon, M.J. Turner, D. Jayatilaka, M.A. Spackman, University of Western Australia, 2012. (b) M.A. Spackman, D. Jayatilaka, *CrystEngComm*, 2009, **11**, 19. (c) M.A. Spackman, J.J. McKinnon, *CrystEngComm*, 2002, **4** , 378, (d) J.J. McKinnon, D. Jayatilaka, M.A. Spackman, *Chem Commun.*, 2007 , 3814.

(21) T. Gunnlaugsson, P. E. Kruger, P. Jensen, J. Tierney, H. D. A. Ali and G. M. Hussey, *J. Org. Chem.*, 2005, **70**, 10875.

(22) (a) SAINT-NT, Version 6.04; Bruker AXS: Madison, WI, 2001. (b) G. M. Sheldrick, Empirical Absorption Correction Program; Universität Göttingen: Göttingen, Germany, 1996.

(23) A. D. Becke, *J. Chem. Phys.*, 1993, **98**, 5648.

(24) Gaussian 09, Revision A.02, M. J. Frisch, G. W. Trucks, H. B. Schlegel, G. E. Scuseria, M. A. Robb, J. R. Cheeseman, G. Scalmani, V. Barone, B. Mennucci, G. A. Petersson, H. Nakatsuji, M. Caricato, X. Li, H. P. Hratchian, A. F. Izmaylov, J. Bloino, G. Zheng, J. L. Sonnenberg, M. Hada, M. Ehara, K. Toyota, R. Fukuda, J. Hasegawa, M. Ishida, T. Nakajima, Y. Honda, O. Kitao, H. Nakai, T. Vreven, J. A. Montgomery, Jr., J. E. Peralta, F. Ogliaro, M. Bearpark, J. J. Heyd, E. Brothers, K. N. Kudin, V. N. Staroverov, R. Kobayashi, J. Normand, K. Raghavachari, A. Rendell, J. C. Burant, S. S. Iyengar, J. Tomasi, M. Cossi, N. Rega, J. M. Millam, M. Klene, J. E. Knox, J. B. Cross, V. Bakken, C. Adamo, J. Jaramillo, R. Gomperts, R. E. Stratmann, O. Yazyev, A. J. Austin, R. Cammi, C. Pomelli, J. W. Ochterski, R. L. Martin, K. Morokuma, V. G. Zakrzewski, G. A. Voth, P. Salvador, J. J. Dannenberg, S. Dapprich, A. D. Daniels, O. Farkas, J. B. Foresman, J. V. Ortiz, J. Cioslowski, and D. J. Fox, Gaussian, Inc., Wallingford CT, 2009.

(25) A. D. Becke, *Phys. Rev. A*, 1988, **38**, 3098.

(26) C. Lee, W. Yang and R. G. Parr, *Phys. Rev. B*, 1988, **37**, 785.